Bistable Phase Behavior and Kinetics of Nonisothermal Mesophase Formation in a Chiral Side Chain Polymethacrylate

Mikhail Kozlovsky,*,† Berndt-J. Jungnickel,‡ and Helmut Ehrenberg§

Institute of Macromolecular Chemistry, Darmstadt University of Technology, Darmstadt, Germany; German Institute for Polymers (DKI), Darmstadt, Germany; and Institute of Material Science, Darmstadt University of Technology, Darmstadt, Germany

Received November 17, 2004; Revised Manuscript Received January 23, 2005

ABSTRACT: Nonisothermal kinetics of smectic phase formation in a chiral liquid crystalline (LC) azodye polymer is studied. The Ozawa exponent value of $n \sim 2.5$ is estimated for narrow polymer fractions with $M_w/M_n \sim 1.3-1.6$ but a temerature-dependent value, $0.5 < n < 1.2$, for the raw polymer of $M_w/M_n \sim 2.6$. The effect of molar mass on mesomorphism is studied, and the dependence of melting temperature on subsequent heating from the rate of previous cooling, r, is theoretically explained. The narrow fractions show a "bistable" phase behavior forming conventional Sm A phase on slow cooling, $r < 1$ K/min, but another (probably a highly twisted TGB A*) mesophase on fast cooling, $r > 1$ K/min. A theoretical model for such a behavior is suggested, and the structure of the two phases is studied by SAXS. The applicability of the Kissinger approach to estimation of activation energy for TGB A* phase formation is discussed.

I. Introduction

The isothermal crystallization of polymers is well described[1,2] and is usually interpreted in terms of the Avrami approach. The theory developed by Mel Avrami as early as in the 1940s[3,4] considers a tiny nuclei of a new phase continuously created or existing within the old phase. There is a time-dependent probability of nuclei activation for their growth, and not yet activated nuclei start to grow later or will be swallowed by the growing phase.

The Avrami equation

$$1 - \xi(t) = \exp(-Bt^k) \tag{1}$$

describes growth of the volume part of the new phase, ξ, as a function of time, t. For a given substance and crystal habit, there is an "isokinetic range" of temperatures and concentrations throughout which the kinetics of phase transformation in the characteristic time scale remains unchanged. The original theory yields integer k values from 1 (linear growth of crystal nuclei) through 2 (two-dimensional growth) to 3 and 4 for spherical crystallization, depending on the mode and dimensionality of nucleation. The Avrami analysis was successfully applied to the crystallization of polymers from LC phases,[5−8] to the growth of mesophases from isotropic polymer melts,[9−13] and to phase transition between polymer LC phases as well.[14,15]

Isothermal studies are however possible only when the phase transformation rate is much larger than thermal response of the measuring system. Moreover, it does not apply to practical processes such as industrial synthesis or device fabrication which proceed under nonisothermal conditions. For that case, Ozawa[16] has extended the Avrami approach to the situation of polymer heating/cooling at a constant rate. The Ozawa equation is written as

$$1 - \xi(T) = \exp(-\Phi(T)r^n) \tag{2}$$

where r is the cooling rate, $\Phi(T)$ is called the cooling function of the process, and the Ozawa exponent, n, depends again on the domain growth and nucleation mechanism. Similar to the Avrami plot, the Ozawa plots in coordinates $\ln\{-[1 - \ln \xi(T)]\}$ vs $\ln(r/\mathrm{K\ min^{-1}})$ should show a series of parallel straight lines, thus corresponding to an "isokinetic" mode of phase transformation. To date, the Ozawa analysis is widely used to decribe nonisothermal crystallization of industrial polymers.[17−20]

In this work, we have used the Ozawa approach to study the mesophase formation in a chiral side chain azo dye polymethacrylate, P8*NN

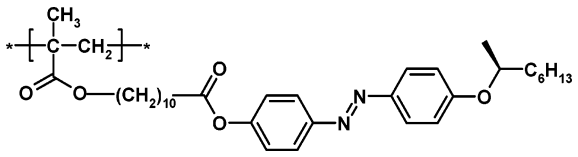

for both raw polymer and its narrow fractions of different molar mass. The recently synthesized polymer is distinguished for high photooptical response being a promising holographic media. Thus, e.g., a phase holographic gitter written in a P8*NN film by circularly polarized laser beam shows diffraction efficiency as high as 35% and more.[21]

The mesophase of the polymer, as formed by spontaneous cooling from above the phase transition, appears optically isotropic and transparent for the wavelength range $\lambda > 500$ nm but possesses a hidden layered (smectic) structure. On the other hand, an ambiguous mesomorphism has been observed for P8*NN so that its optical appearance as an LC glass depends critically on cooling rate. For that reason, the kinetics of mesophase formation in the polymer and the effect of molar

† Institute of Macromolecular Chemistry, Darmstadt University of Technology.
‡ German Institute for Polymers.
§ Institute of Material Science, Darmstadt University of Technology.

10.1021/ma047631o CCC: $30.25
Published on Web 03/08/2005

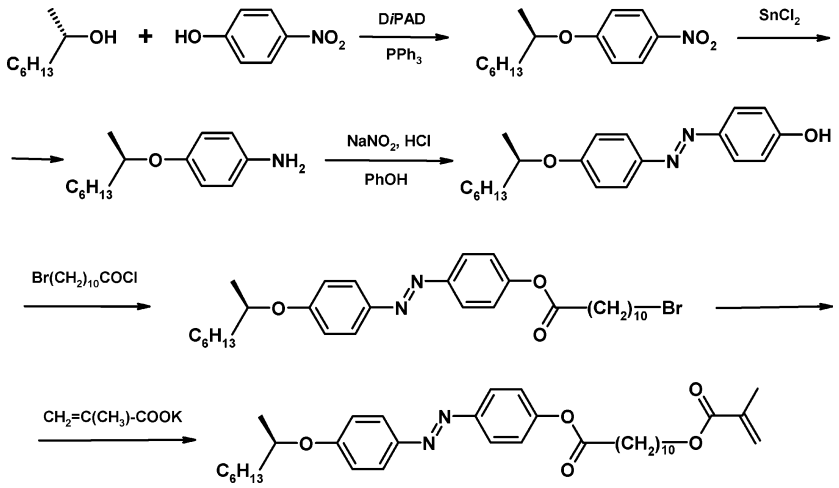

Figure 1. Synthesis of the monomer M8*NN.

mass distribution as treated in this paper are of great importance.

II. Experimental Section

1. Synthesis of the Monomer. The monomer M8*NBN was synthesized according to the scheme in Figure 1.

***p*-[2-(*S*)-Octyloxy]nitrobenzene.** The R(+)-2-octanol (10 g, 76.8 mmol), *p*-nitrophenol (11 g, 79 mmol), and diisopropyl azodicarboxylate (16 mL, 79 mmol) were dissolved in 350 mL of ether and cooled in a water−ice bath for 0.5 h, and then the solution of the triphenylphosphine in 50 mL of ether was added dropwise during 5 min with stirring. The mixture was stirred at room temperature overnight, the precepitate filterred off, and the solvent removed. Since removal of the ether induced further precipitation, the procedure was repeated five times with 3−4 h intervals, giving a total of 21.8 g of crystalline solid. The solvent was then removed, the rest chromatographed on silica (toluene), and the first fraction collected as a viscous yellowish oil.

Yield: 17.1 g (68 mmol, 90%). $[\alpha]_D = -7.4°$ (0.01 mg/mL in methylene chloride). ^{1}H NMR (ppm): 8.19 (d, 2H) and 6.92 (d, 2H) aromatic, 4.48 (hx, 1H) −O−C*H(CH$_3$)−C$_6$H$_{13}$, 1.78 (m, 1H) and 1.65 (m, 1H) −O−C*H(CH$_3$)−CH_2−C$_5$H$_{11}$, 1.2−1.5 aliphatic including 1.36 (d, 1H) −O−C*H(CH_3)−C$_6$H$_{13}$, and 0.91 (t, 3H) −O−C*H(CH$_3$)−C$_5$H$_{10}$−CH_3.

***p*-2-(*S*)-Octyloxyaniline.** 65 g (0.29 mol) of $SnCl_2$ was suspended in ethanol, 14.3 g (57 mmol) of the *p*-2-(*S*)-octyloxynitrobenzene added, and the mixture refluxed under nitrogen for 1 h. After cooling, the reaction mixture was poured into ice water. The solution pH was turned slightly basic (7−8) by addition of solid K_2CO_3. The product was extracted with ether, washed with brine, and dried with anhydrous $MgSO_4$. The solvent was distilled off, and from 12.1 g of crude product, the aniline was distilled at reduced pressure as a yellow oil; bp 132−134 °C at 5 mmHg. Yield: 11.1 g (50 mmol, 88%).

***p*-2(*S*)-Octyloxy-*p*′-hydroxyazobenzene.** 9.6 g (43 mmol) of *p*-2-(*S*)-octyloxyaniline was dissolved in 40 mL of ethanol, 40 mL of 6 N HCl added, the ethanol removed under vacuum at 40 °C, and the rest left overnight at +4 °C. An ivory solid crystallized over the acid aqueous solution. The solid was powdered, cooled to 0 °C in an ice−salt bath, and an additional 20 mL of HCl added; the solution of 2.9 g (42 mmol) of $NaNO_2$ in 20 mL of water was added dropwise with stirring, keeping the temperature not above +5 °C (solution 1).

Phenol (4.0 g, 42 mmol) was dissolved in 100 mL of 2 N NaOH and cooled to 0 °C in an ice−salt bath (solution 2). Then solution 1 was added dropwise with stirring, keeping the temperature not above +5 °C. After all solution 1 added, the mixture was stirred overnight at room temperature. The reaction media was then extracted with 4 × 200 mL of ether, washed with water, and dried over $MgSO_4$. The rest after evaporation of ether was chromatographed on silica twice, the first time changing the eluant from pure toluene to a toluene−ethyl acetate 4:1 mixture and the second time with 10% ethyl acetate in hexane. The goal product after removal of the solvent in vacuo appears as a cherry viscous oil. Recrystallization from hexane at −18 °C gives an orange solid with melting point below ambient temperature. Yield: 11.9. g (33 mmol, 75%).

***p*-11-Bromoundecanoyloxy-*p*′-2-(*S*)-octyloxyazobenzene.** 19.1 g (33 mmol) of *p*-2-(*S*)-octyloxy-*p*′-hydroxyazobenzene, and 5 mL (3.7 g, 36 mmol) of triethylamine were dissolved in 100 mL of dry ether, and the solution of 12 g (42 mmol) of ω-bromoundecanoyl chloride in 50 mL of ether was added dropwise (immediate precepitation of triethylammonium chloride observed). The reaction media was stirred overnight, then washed with water, diluted HCl, and water again, and dried over $CaCl_2$. The solvent was evaporated in vacuo, and the residue was chromatographed on silica (toluene) and recrystallized from ether to hexane, giving the goal ester as egg-yellow plates. Yield: 9.0 g (15.6 mmol, 50%); mp 81 °C. ^{1}H NMR (ppm): 7.88 (d+d, 4H), 7.21 (d, 2H), and 6.98 (d, 2H) aromatic; 4.46 (m, 1H) −O−C*H(CH$_3$)C$_6$H$_{13}$; 3.45 (t, 2H) Br−CH_2−CH$_2$−; 2.58 (t, 2H) −CH$_2$−CH_2−COO−; 0.9−1.9 aliphatic.

***p*-11-Methacryloyloxyundecanoyloxy-*p*′-2-(*S*)-octyloxyazobenzene.** 6.5 g (11.2 mmol) of the bromo precursor was dissolved in 50 mL of freshly distilled 1,3-dimethylimidazolidinone-2, and 3 g (24 mmol) of powdered potassium methacrylate was added. The mixture was stirred at room temperature for 24 h and then poured into 300 mL of ice water, filtered, dissolved in ether, washed with water, and dried over $CaCl_2$. The solvent was removed, and the rest was chromatographed, changing eluent from the toluene−hexane 1:1 mixture through pure toluene to the toluene−ethyl acetate 19:1 mixture. The product recrystallized from methanol (mp 44.5 °C), but the monomer can be supercooled and crystallizes at arbitrary temperature, as e.g. 34 °C under shear flow. Yield: 4.5 (7.7 mmol, 70%). ^{1}H NMR (ppm): 7.9 (d+d, 4H), 7.2 (d, 2H), and 7.0 (d, 2H) aromatic; 6.1 (s, 1H) and 5. (s, 1H) CH_2=C(CH$_3$)−COO−; 4.5 (m, 1H) −O−C*H(CH$_3$)C$_6$H$_{13}$; 4.2 (t, 2H) OOC−CH_2−CH$_2$−; 2.6 (t, 2H) −CH$_2$−CH_2−COO−; 1.9 (s, 3H) CH$_2$=C(CH_3)−COO−; 0.9−1.7 aliphatic.

2. Polymerization and Fraction Separation. The chiral methacrylic azo dye polymer P8*NN was prepared by radical polymerization of its monomer in solution, as follows. The monomer (4.0 g, 6.9 mmol) and AIBN (40 mg, 0.24 mmol) were dissolved in 40 mL of toluene, bubbled 0.5 h with Ar, and then ampule closed and kept at 60 °C for 65 h. Then the solution was diluted with toluene to 100 mL, and 45 mL of methanol was added. The turbid liquid was heated until complete clearing and let stay overnight at room temperature. The mother liquid was carefully decanted, and the sediment (bottom layer) was dried in vacuo, giving fraction I. The procedure was repeated with the mother liquid six times more by adding 10 mL of methanol, each time giving fractions II−

Table 1. Molar Mass Parameters for the P8*NN Fractions

polymer	av molar mass, M_w (10^4 g/mol)	av deg of polymerization, p_w	dispersion ratio, $D = M_w/M_n$
fraction I	9.29	160	2.04
fraction II	5.45	94	1.56
fraction III	4.02	69	1.41
fraction IV	3.05	53	1.36
fraction V	2.33	40	1.28
fraction VI	1.66	28	1.21
fraction VII	1.1	19	1.17
raw polymer	2.9	50	2.63

VII, respectively. The nonfractioned raw polymer sample was obtained by a separate polymerization of 0.3 g of monomer; the sample was three times reprecipitated from toluene to methanol and six times washed with boiling methanol.

Molar masses and dispersion ratios for the polymer fractions are listed in Table 1.

3. Measurements. The molar mass of the polymer fractions was estimated by size exclusion chromatography (SEC) in THF solution using PMMA as standard.

DSC curves were taken using Perkin-Elmer DSC-2C equipment calibrated with indium standard. The transition temperatures were estimated on heating as DSC peak maximum but on cooling as crossing of baseline with tangent of the ascendent peak wing. The values estimated in this way have been shown to correlate in a best way with the transition temperatures observed by polarization microscopy (for the birefringent phase state, Sm A).

X-ray diffraction profiles within the whole range ($0.9° < 2\Theta < 29°$) from 1 mm diameter capillary samples were recorded on a STOE four-circle diffractometer with graphite monochromatized Cu Kα radiation, $\lambda = 1.54$ Å, but precise SAXS measurements ($0.6° < 2\Theta < 10°$) with Co Kα radiation, $\lambda = 1.7902$ Å. Two-dimensional X-ray diffraction data have been collected from an isolated fiber (18 μm diameter), using the single-crystal diffractometer Xcalibur from Oxford Diffraction. Mo Kα radiation was monochromatized by a pyrolytic (002) graphite crystal, and data were recorded by the sapphire CCD detector for a sample-to-detector distance of 6 cm. 180 frames were collected in φ-scan mode in steps of 1° with the rotation axis parallel to the fiber and perpendicular to the incident beam.

Polymer films and X-ray samples with predetermined thermal history were prepared using the STC200/HS400 programmable heating stage (INSTEC).

III. Results and Discussion

1. Bistable Phase Behavior. It is well-known that the phase transition behavior of crystallizable polymers can be affected by thermal history. Thus, e.g., melting temperature grows roughly linearly with the temperature of previous isothermal crystallization,[22] as expressed by an evaluation procedure derived by Hoffman and Weeks.[23] The effect is of significant importance especially for LC polymers (LCPs) which can form a variety of mesophases between crystal or glass and isotropic liquid melt. We have already reported some cases when thermal pretreatment and particularly cooling rate change phase behavior of an LCP not just quantitatively (transition temperature) but also qualitatively (sequence of mesophases).[15,24]

All the P8*NN fractions I−VII show a prominent difference in optical appearance if cooled from above the transition point fast (10 K/min) or slowly (1 K/min). When cooled fast, the polymer film at ambient temperature is transparent and optically isotropic. Contrarily, slow cooling results in films that are both birefringent and turbid, as illustrated in Figure 2 for an about 20 μm thick film of fraction I with the highest molar mass.

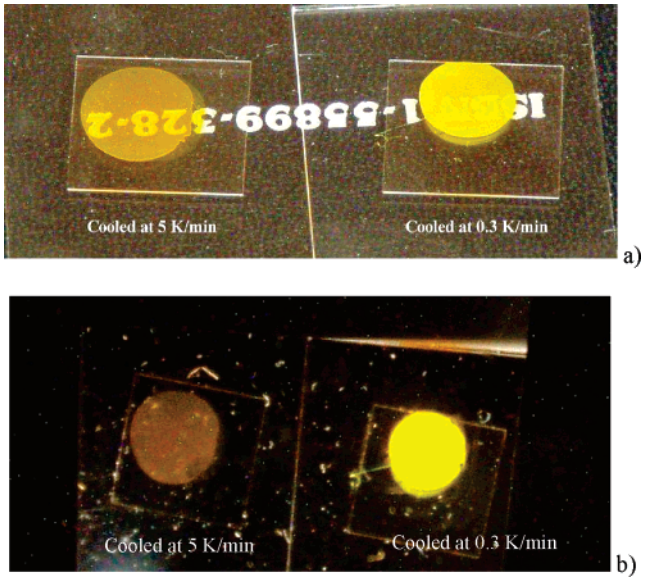

Figure 2. Optical appearance of a P8*NN, fraction I film cooled at different rates: (a) daylight, no polarizers; (b) crossed polarizers.

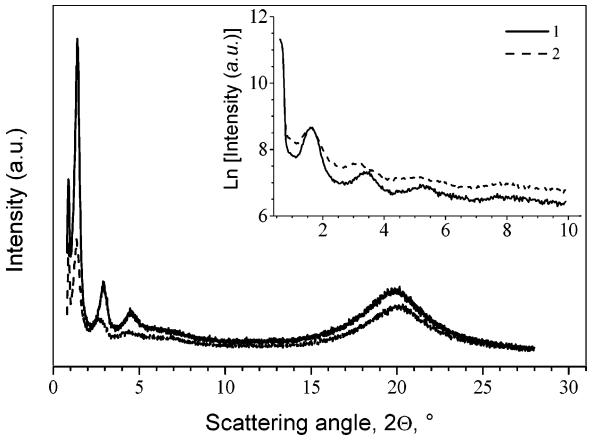

Figure 3. One-dimensional X-ray scattering profiles from P8*NN fraction I at room temperature: 1, in the turbid phase state (Sm A, cooled 0.3 K/min); 2, in the transparent phase (probably TGB A*, cooled 10 K/min). Insert: small-angle scattering range, on a logarithmic scale.

A careful study of thermal behavior of the raw P8*NN has shown the same bistable phase behavior as for its fractions but at much lower critical cooling rates, r: the polymer film can also form a "turbid" Sm A texture but after cooling not faster than 0.3 K/min only.

Identification of the both mesophases and elucidation of structural difference between those is of great importance for the work. On the other hand, a detailed discussion on that topic is far beyond the goals and the scope of our paper, which is devoted mostly to the kinetics of mesophase formation. For that reason, we will discuss the obtained structural data shortly presenting the basic results, and a detailed structural study of the polymer will be published elsewhere.

One-dimensional X-ray scattering profiles from the two mesophases are shown in Figure 3, and the data on scattering reflections are summarized in Table 2. It is worth noticing that the presented results correspond to the same sample at the same temperature but after different thermal pretreatment. Both mesophases show a set of three SAXS peaks which more or less correspond to three reflection orders from a single lattice.

Table 2. Reflection Positions for P8*NN (Fraction I) in Two Different Phase States (25 °C)

mesophase	small-angle reflections			wide-angle reflection	width of the WAXS reflection
	$d_1 \pm 1.5$ (Å)	$d_2 \pm 1.0$ (Å)	$d_3 \pm 0.5$ (Å)	$D \pm 0.01$ (Å)	$\text{fwhm}_D \pm 0.05$ (deg)
SmA	61.8	30.3	19.6	4.47	4.54
TGBA*	64.8	33.0	20.2	4.32	4.82

The data indicate a minor but significant diference in a smectic layer organization of the two phases. The "turbid" mesophase of P8*NN is characterized by somewhat more ordered and more compact layer packing, as evidenced by smaller d_1 spacing value and by narrower wide angle scattering halo (fwhm_D values). The width of the wide angle peak is nevertheless much higher than would be characteristic for more ordered smectic phases, such as Sm B.

Generally, microscopic observations and X-ray data support the smectic A structure of the "turbid phase". The calculated length of the mesogenic group is about 37.3 Å (the corresponding molecular model is shown in the Supporting Information, Figure S1). Therefore, a bilayer packing of mesogens can be suggested with overlapping of neighboring layers up to aromatic cores (shown schematically in Supporting Information, Figure S2). An alternative model of a bilayer Sm C* structure with a tilt angle of about 30° is excluded by absence of any ferroelectric properties in the substance.

The nature of the "transparent" mesophase is less clear. It should possess a similar type of Sm A ordering but be more defective. At the same time, the lack of visually observed birefringence should be somehow explained.

For conventional liquid crystals, the absence of birefringence in a particular direction can be observed in specially prepared oriented monodomain samples only but not in bulk, nor in spheric drops at an arbitrary direction, as for P8*NN. We should comment first that such a visually isotropic mesophase with a hidden smectic ordering was never observed by nonchiral polymers of a similar structure, as e.g. LC poly(meth)acrylates with azobenzene photochromic side chains.[11,25−28] On the other hand, we have reported similar mesophases for numerous chiral homopolymers (polymethacrylates, polysiloxanes)[29−32] and their copolymers with nonchiral azodye comonomers.[24,33,34] The detailed study of the "transparent smectic mesophase" is presented in our recent paper;[32] here we will summarize them briefly.

(i) The smectic ordering in the mesophase is evidenced by DSC data, X-ray measurements, and broad-line NMR spectra.

(ii) For colorless chiral LC polymers, the presence of a short-pitch helical superstructure is proven by UV absorption and, more importantly, by UV reflection spectra in thin films and also by circular dichroism (CD) and by optical rotatory dichroism (ORD) spectra. The helical pitch is estimated to be as short as 240−250 nm, i.e., out of the visible wavelength range. For azo dye copolymers, any measurements above are impossible because of strong absorption of the photochromic moieties.

(iii) AFM profiles of a free polymer surface also give evidence of a two-dimensional periodic structure with a ~0.25 μm spacing. Worth noticing is that such a profile has been measured for an azo dye chiral copolymer.[35]

(iv) Chirality is critical for the formation of such a mesophase. Thus, the sign of optical rotation corresponds to the absolute configuration of chiral centers in mesogenic groups. Also, enantiomeric copolymers composed of the two optically isomeric monomers do form the "transparent" phase up to a certain value of enantiomeric excess only, while racemic copolymers form the conventional Sm A phase instead.

The only structural model which can explain the whole combination of the experimental data remains to date an extra short pitch TGB (twist grain boundary) phase, namely TGB A*.

It is well-known that a uniform helical twisting in a smectic A phase composed of chiral molecules is forbidden by symmetry rules. To overcome the frustration, small Sm A blocks in the TGB phase form a discontinuous helical superstructure via a three-dimensional lattice of screw disclinations penetrating the whole phase.[36] A sketch of the TGB A phase is shown in the Supporting Information (Figure S3). The TGB phases in low molar mass liquid crystals appear in a short temperature range above the Sm A phase, and they are birefringent and can show selective reflection of visible light.[37] In contrast, the "transparent smectic" phase of chiral polymers show a remarkable stability over temperature and can be frozen in glass. In this connection we should mention the early publications of Freidzon et al.[38] on cholesterol-containing poly(meth)acrylates which reveal a helical twisting along with the selective light reflection in the Sm A phase, also in a broad temperature range. Stabilization of the TGB-like stucture by the polymer main chain penetrating the screw defect system might be the reason for such a thermal behavior. However, we have reported earlier a TGB A* → Sm A transition in chiral azo dye copolymers which can be observed at low cooling rates only, $r < 1$ K/min.[24]

For the particular case of the "transparent smectic" mesophase, an extra-short helical pitch of ~250 nm or less has been suggested, so that all structural elements of the phase are smaller in dimensions than wavelength of visible light. Hence, neither birefringence nor light scattering at domain boarders can be observed visually even for 15−30 μm thick films, as used for microscopic observations.

The exact TGB A* structure for P8*NN fractions can be hardly proven experimentally. It has been reported[36] that any reliable and convincing information on the TGB A* phase can be obtained only by high-resolution X-ray scans from well-aligned samples. Generally, orientation of LC polymers is a complicated experimental task, as compared with orientation of low molar mass liquid crystals. For the particular case of P8*NN, the orientation cannot be produced by extremely slow cooling in a magnetic field, while another phase state (Sm A) will be formed instead. We have tried to orient a thin polymer fiber by drawing it from the isotropic melt above the phase transition. Such a 18 nm thick fiber shows a remarkable birefringence (Supporting Information, Figure S4), but no splitting of the outer X-ray reflection (Supporting Information, Figure S5), probably to insufficient orientation.

To summarize, the short pitch TGB A* structure for the "transparent smectic" mesophase of P8*NN is not proven conclusively yet remains the most probable one.

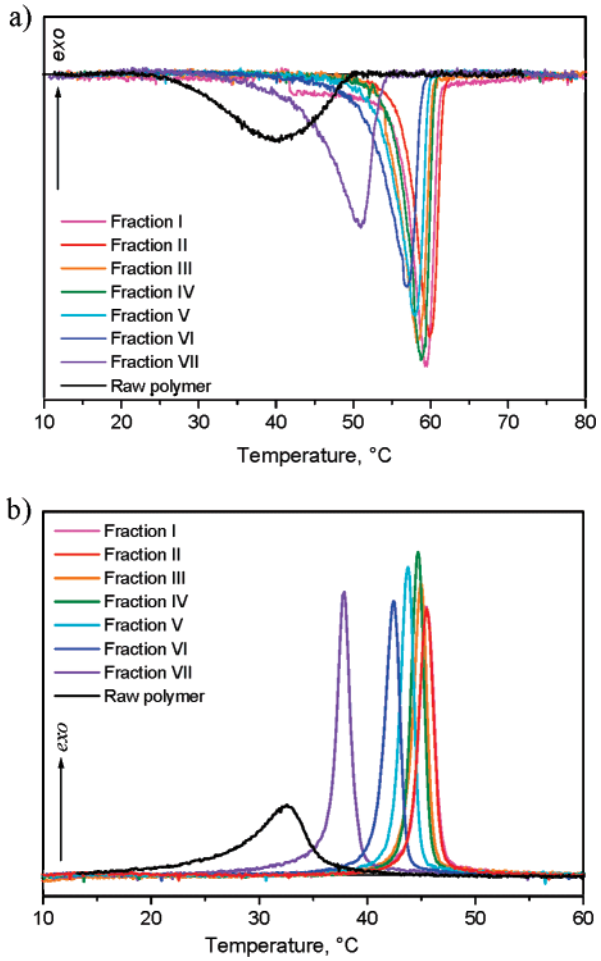

Figure 4. DSC scans from P8*NN fractions, normalized to sample weight: (a) second heating; (b) second cooling.

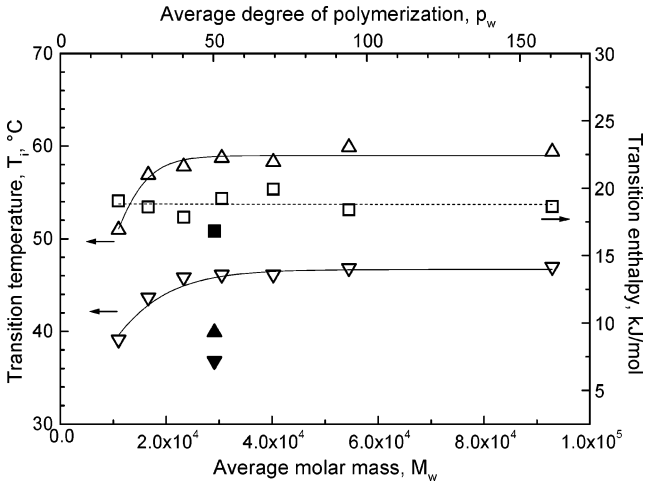

Figure 5. Phase transition temperatures on heating (T_m, ▲), and on cooling (T_c, ▼,) and melting enthalpies, ΔH_m (■), for the P8*NN fractions (open symbols) and raw polymer (closed symbols), vs average molar mass, M_w.

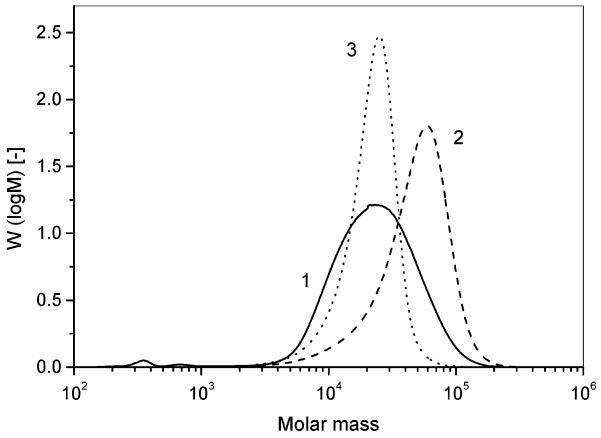

Figure 6. SEC profile from raw P8*N and its fractions II and V.

The X-ray data of Figure 3 and Table 2 also confirm some "deteriorated Sm A" structure of the phase. For that reason, we suggest the given structure for the "transparent phase state" of P8*NN fractions.

2. Nonisothermal Mesophase Formation. DSC curves from the P8*NN fractions are shown in Figure 4. The second heating/cooling scan at 10 K/min was chosen to represent the thermal behavior since heating above the transition point, T_m, erases any effect of previous thermal treatment (all the subsequent heating/cooling scans without any annealing show the same curve). It can be clearly seen that the phase transition for the raw polymer occurs in a broad temperature range and about 15−20 K lower than for its fractions with narrower molar mass distribution.

The transition temperatures for the polymer fractions on heating, T_m, and on cooling, T_c, are plotted against the average molar mass, M_w, in Figure 5 along with the transition enthalpies, ΔH_m. For the sake of comparison, also data for the raw polymer are shown. The data of Figure 4 show that both T_m and T_c values become independent of the molar mass starting from the average degree of polymerization, $p_w \sim 30$. Thus, fraction VII can be considered rather as an oligomer but all other fractions as true polymers. At the same time, the raw polymer shows about 20 K lower transition temperature on heating, as compared with fraction IV of similar molar mass, $M_w \sim 3 \times 10^4$ g/mol. A less pronounced but nevertheless remarkable difference of about 10 K is observed also for the cooling scan. Such a difference can be hardly explained by a broader dispersion ratio only, $D = 2.6$ for the raw polymer vs $D = 2.04$ for fraction I, but rather by the presence of small amounts of the monomer in the raw P8*NN, as indicated by original GPC−SEC data shown in Figure 6. At the same time, the transition enthalpy, ΔH_m, shows no influence of molar mass value at all.

When cooling the sample at different rates, the DSC peak shifts toward lower temperatures with increasing rate, r, as illustrated by Figure 7 for fraction II. The dependence of the peak maximum position on cooling rate is however qualitatively the same for raw P8*NN and all the fractions (some examples shown in Figure 8a). We should note here that estimation of the transition enthalpy from DSC curves for slow cooling is rather complicated, since improper adjustment of the baseline leads to high experimental errors. Nevertheless, rough evaluation shows that the ΔH_m value is independent of the cooling rate, as shown in Figure 9 for the particular example of fraction IV.

As seen from Figure 4, the DSC peak for the raw polymer is much broader than for the fractions. To quantify that, we can define the transition interval as difference between temperatures corresponding to conversion rates of 10% and 90%, correspondingly

$$\Delta T_{10/90} = T_{\xi=10} - T_{\xi=90}$$

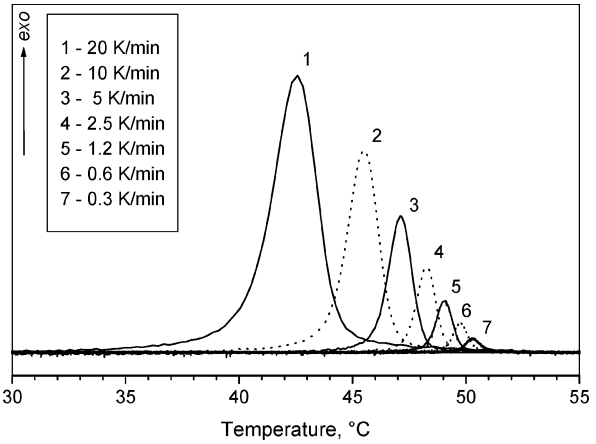

Figure 7. DSC scans from P8*NN, fraction II, at different cooling rates.

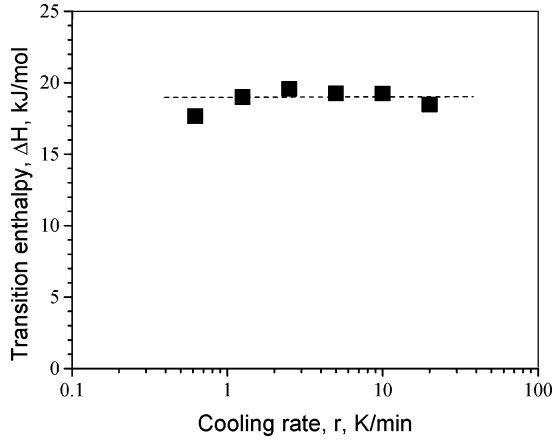

Figure 9. Transition enthalpy on cooling, T_c for P8*NN fraction IV, vs cooling rate.

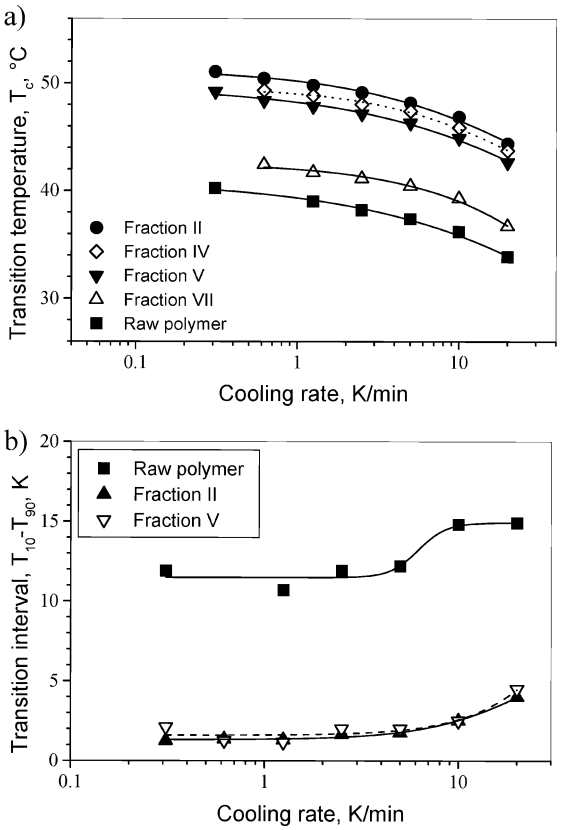

Figure 8. Transition temperature on cooling, T_c (a), and phase transition interval, $\Delta T_{10/90}$ (b), for raw P8*NN and its fractions, vs cooling rate.

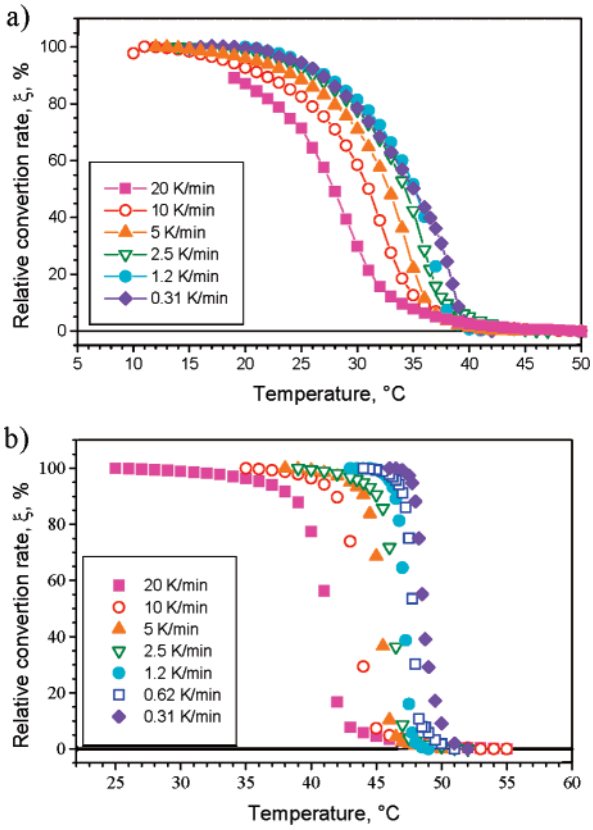

Figure 10. Development of the short pitch TGB A* mesophase in raw P8*NN (a) and its fraction V (b) vs temperature on cooling at different coooling rates.

the value appears to be the same for both fractions, II and V (as e.g. 2.5 K for the standard cooling rate of 10 K/min) but an order of magnitude higher for the nonfractioned polymer (15 K, correspondingly), as shown in Figure 8b. This may have the same origin as the strong deviation in the transition temperatures themselves, i.e., the presence of small amounts of the monomer.

For the detailed kinetic studies, fractions II and V were chosen along with the raw polymer. The phase transformation rate, $\xi(t)$, is calculated by integration of the DSC curves upon temperature, as shown in Figure 10 for the raw P8*NN sample and fraction V.

The Ozawa plot for raw P8*NN is presented in Figure 11a and that for its fraction V in Figure 11b (fraction II shows qualitatively similar behavior). There are however certain experimental problems in plotting the data of Figure 9 in Ozawa coordinates, $\ln\{-[1 - \ln \xi(T)]\} - \ln(r/\mathrm{K\ min^{-1}})$. First, the experimental error in ξ values grows drastically, as cooling rate decreases. Second, the Ozawa value, $\ln\{-[1 - \ln \xi(T)]\}$, is especially sensitive to proper choice of the baseline position. For that reason, only the middle part of the $\xi(T)$ curves in Figure 10 ($0.05 < \xi < 0.95$) can be used for further calculations. Also, the narrow temperature ranges of the transition, as observed for polymer fractions (Figure 8b) do not overlap enough (Figure 10b), to allow the Ozawa analysis in the whole range of cooling rates, r, measured, in contrast to the raw polymer.

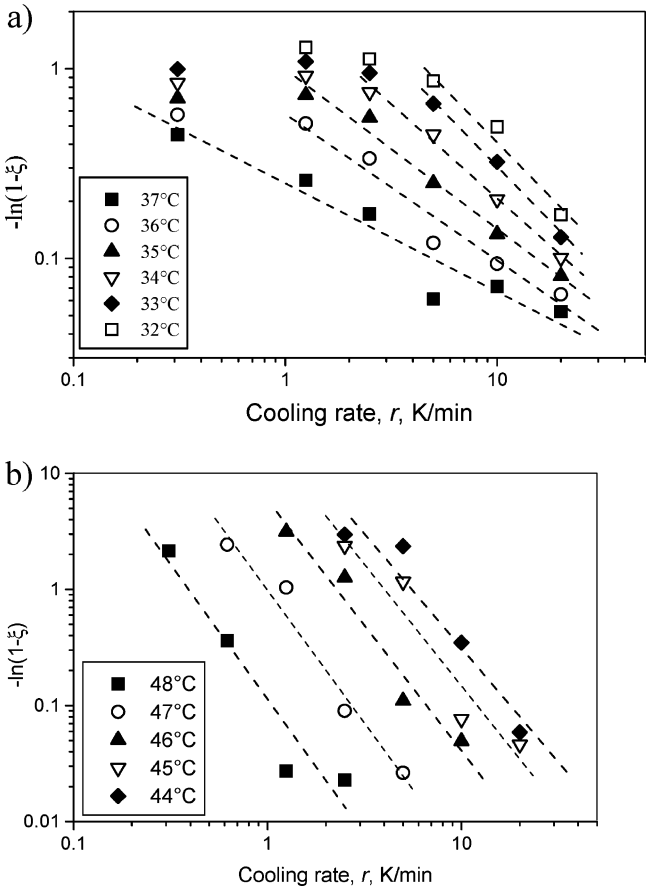

Figure 11. Ozawa plots for the kinetics of mesophase formation in raw P8*NN (a) and its fraction II (b) at different temperatures.

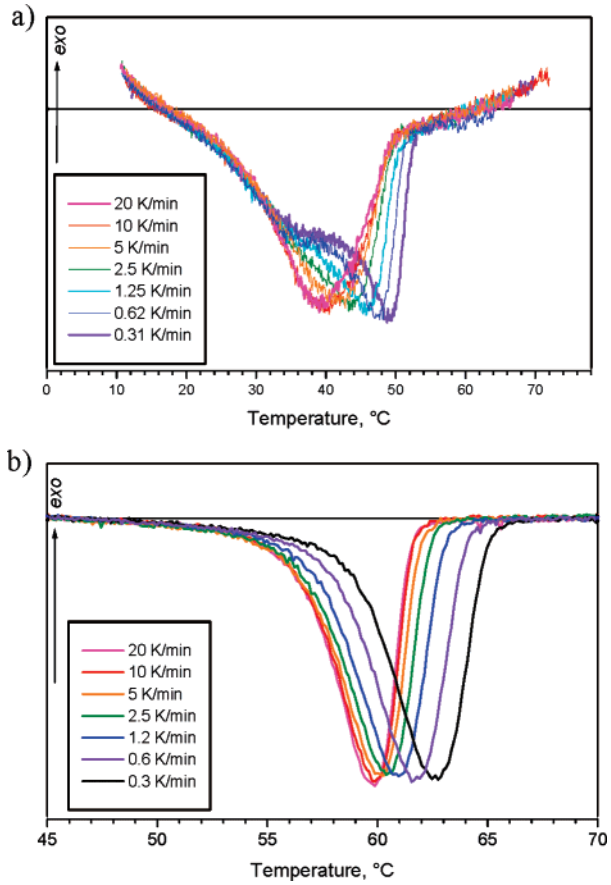

Figure 12. DSC curves on heating at 10 K/min from raw P8*NN (a) and its fraction II (b) cooled previously at different rates.

Taking that in mind, we can conclude that the polymer fractions behave in any case according to the Ozawa theory (Figure 11b). In contrast, the kinetic data for the raw polymer (Figure 11a) fall to straight lines in Ozawa coordinates only at high temperatures and high cooling rates; the lower the temperature, the higher is cooling rate value, r, where deviation from the straight line begins. The considerations above justify however the neglection of the measuring points at lower cooling rates as not representative, and the remaining points allow again a satisfactory Ozawa analysis.

Before doing that, however, we should return to the utmost example of the different phase growth at fast and slow cooling of the polymer, namely the bistable phase behavior (as discussed in the previous section). Influence of the cooling rate on the phase condition of P8*N can be observed also by DSC. Figure 12 presents DSC scans from raw P8*NN (a) and its fraction II (b) at standard heating rate of $r = 10$ K/min but after the sample having been cooled at different rates. As seen from the figure, the transition point on subsequent heating, T_m, shifts to higher temperatures as the cooling rate decreases.

For the raw polymer, also a threshold at ~25 °C can be much better observed at the lowest rates of previous cooling. Neither polarization microscopic observation nor X-ray studies show any changes in the polymer film at that temperature, however. For that reason, we would suggest the threshold indicating rather partial devitrification of the polymer than a Sm A−TGB A* phase transition. The detailed structural studies are in progress and will be published elsewhere.

Qualitatively, the data of Figure 12 can be easily explained by larger domain size for lower cooling rates, similar to crystallization and subsequent melting of crystallizable polymers.[22] However, quantitatively the effect of cooling rate seems to be more complicated. When T_m values plotted against logarithm of the rate of previous cooling, r, the data fall to a single straight line for the raw P8*NN (Figure 13a) but not for narrow fractions II and V (Figure 13b) where a kink is observed at $r \sim 1$ K/min. The latter value corresponds to the critical cooling rate for the crossover from a TGB film to a Sm A one, as observed in the thermooptical experiment (Figure 2).

The linear correlation between T_{max} and ln r can be explained as follows. Hoffman and Weeks[23] have shown that that a linear relation holds between crystallization temperature, T_c, and temperature of subsequent melting, T_m: $T_m = cT_c$. Ozawa[16] assumes that ln $\Phi(T) \sim T$ and ln $\Phi(T) \sim aT + b$. Cazé et al.[39] have shown that then $T_c \sim$ ln r and $T_c = n/a$ ln r. Combining this yields $T_m \sim$ ln r and $T_m = cn/a$ ln r as indicated by Figure 13a. A kink in Figure 13b may then indicate a sudden change in n, a change in c (which can be shown to depend on interfacial energies and nuclei size), or a change in a at that r. It will be shown below that n does not change and that consequently growth and nucleation dimensions remain unchanged. The parameters c and a will however change with transition from the TGB to Sm A mesophase formation.

Such a bifurcation in the phase behavior of P8*NN could be explained by Figure 14. A metastable TGB A* phase would be energetically less preferred than the

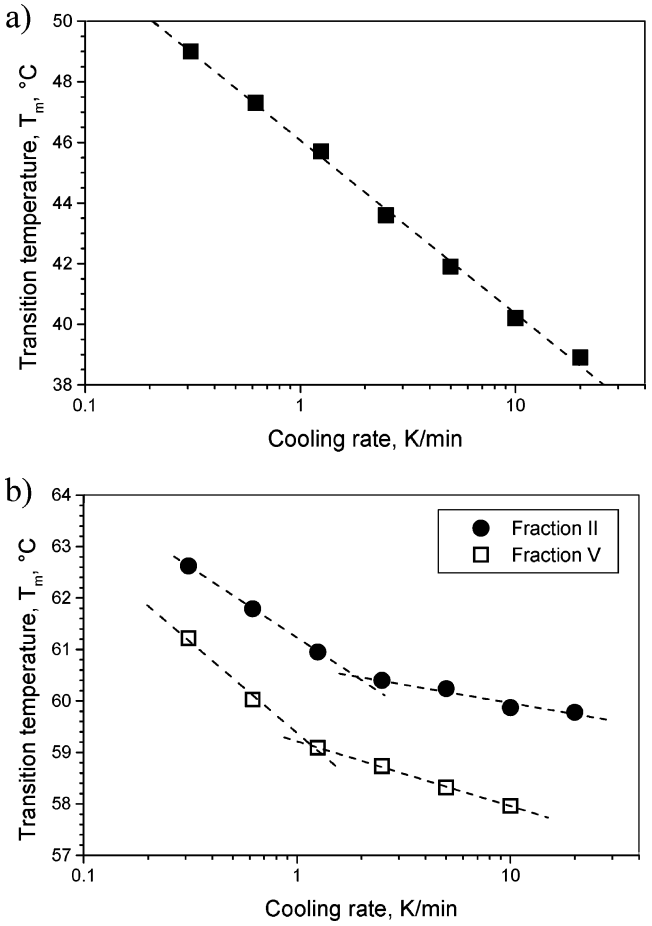

Figure 13. Transition temperature on heating, T_m, for the raw P8*NN (a) and its fractions II and V (b) cooled previously at different rates, vs the cooling rate.

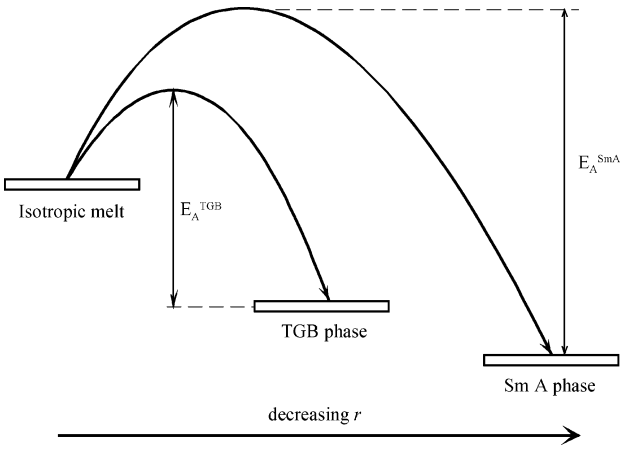

Figure 14. Energy diagram for the bistable phase behavior of P8*NN.

conventional Sm A* phase but requires a lower activation energy barrier to be overcome, $E_A^{TGB} < E_A^{SmA}$.

From our data, only the faster process, namely Iso → TGB A*, can be evaluated and interpreted in terms of Ozawa equation, eq 2. The corresponding Ozawa exponent values, n^{TGB}, and cooling functions, $\Phi^{TGB}(T)$, for raw P8*N and fractions II and V are shown in Figure 15. As seen from the Figures 11 and 15, the exponent values for both polymer fractions are almost independent of temperature, $n^{TGB} \sim 2$. In contrast, the slope of the straight lines changes monotoneously from $n^{TGB} = 0.6$ at 37 °C to $n^{TGB} = 1.2$ at 32 °C for the raw material.

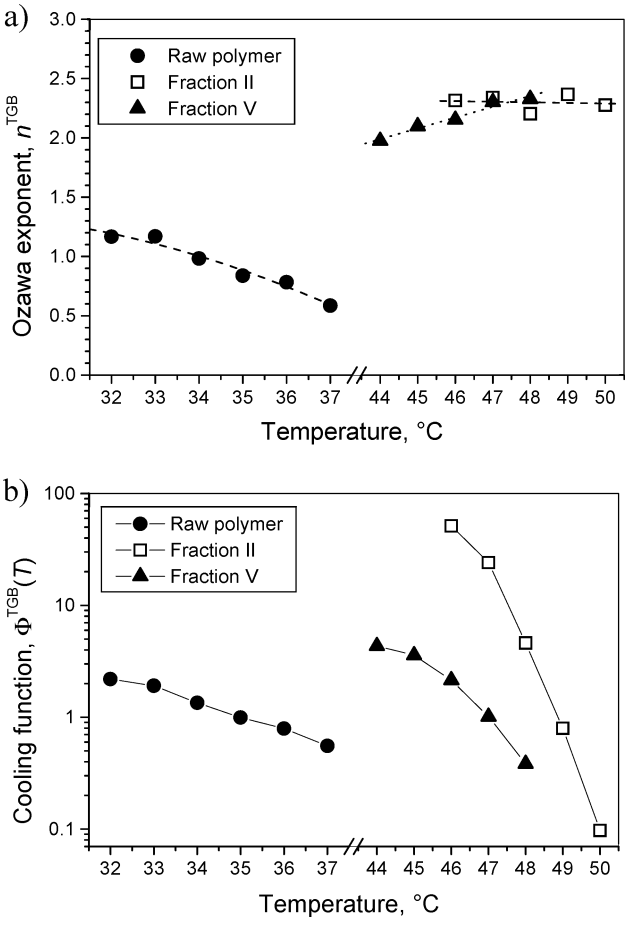

Figure 15. Ozawa exponent values, n^{TGB} (a), and cooling function, $\Phi^{TGB}(T)$ (b), for raw P8*N and fractions II and V, vs temperature.

Interpretation of these figures in terms of nucleation and growth dimensions[20] is however ambiguous since Cheng and Wunderlich[40] have shown that low values of n may hint at nonlinear growth or at a nonnegligible volume fraction of nuclei. In fact, since there is no obvious reason for a change of nucleation and growth dimensions with temperature (except possibly those associated with the transition TGB A* → Sm A), the temperature dependence of n and its small values most probably indicate a temperature-dependent nonlinearity of growth.

Usually, activation energy of the phase formation in polymers is estimated using the Kissinger equation[41]

$$r(T_{max}) = cT_{max}^{2} \exp\left[-\frac{E_A}{RT_{max}}\right] \qquad (3)$$

where R is universal gas constant, c is a preexponential factor, and T_{max} is the DSC peak maximum (as shown in Figure 6a), corresponding to the highest phase transformation rate. The activation energy here is energy required to transport next mesogenic side chains to the growing domain surface.

However, the corresponding Kissinger plots (Figure 16) deviate from the straight lines for both raw P8*NN and its fractions II and V, thus confirming that the mesophase formation in P8*NN cannot be described within a simple Kissinger model.

Note that the sign of the activation energy is negative due to the positive slope of the graphs. In the available literature, that sign problem has always not been

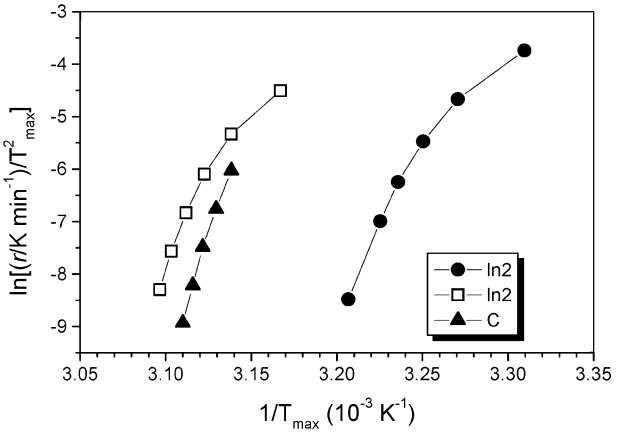

Figure 16. Kissinger plots for estimation of activation energy of the TGBA* phase formation.

considered, with a few exceptions.[42,43] Again, this makes the evaluation ambiguous. Assumed that the sign problem is of negligible importance and the slope yields the activation energy of TGBA* phase nucleation, E_A^{TGB} in Figure 14, we could suggest that the E_A^{TGB} value is not constant but depends on T_{max}, i.e., by virtue of Figure 8a, on the cooling rate. That means that rapid cooling would yield a lower activation energy for the creation of the TGBA* phase. This would be consistent with the experimental finding and the sketch of Figure 14. By reducing the cooling rate, the activation energy increases and finally approaches that for the transition to the Sm A phase which then grows. This argumentation would support the experimental findings and the diagram in Figure 14.

Finally, some speculations could be made about the nucleation in the polymer (following the sketch in Figure 14). The first nucleation phase should be similar for both Sm A and TGB A* phases, i.e., formation of small smectic blocks, about 10 nm in size, i.e., 20−30 mesogenic groups side by side (Supporting Information, Figure S3). When reaching that critical length, there would be a bifurcation point: either the nondisturbed Sm A domain grows further (but that requires a higher activation energy to overcome noncentrosymmetric steric repulsion), or a kink appears, giving rise to the growing screw disclination.

IV. Conclusions

The chiral photochromic LC polymethacrylate P8*NN shows true polymer behavior starting from the average degree of polymerization, $p_w > 25$. On the other hand, the raw (nonfractionized) polymer reveals much broader phase transition at about 20 K lower temperature with $T_{10/90} \sim 12-15$ K, as compared with $T_{10/90} \sim 1-3$ K for fraction V of the same average molar mass. That can be caused by small contamination of the raw polymer with its monomer or dimer. The transition temperature on cooling ("liquid crystallization" temperature, T_c) steadily decreases with increasing cooling rate, r.

The Ozawa plots evidence an isokinetic mesophase growth for polymer fractions; on the other hand, the raw polymer shows deviation from straight lines in Ozawa coordinates at lower temperatures and lower cooling rates.

A crossover from fast formation of transparent, optically isotropic (probably short pitch TGB A*) structure to slow growth of turbid and birefringent Sm A phase has been observed at the critical value, $r \sim 1$ K/min, for narrow polymer fractions but at much slower cooling, $r = 0.3$ K/min, for the raw polymer. A theoretical model for the effect of "bistable phase behavior" has been suggested as the metastable TGB A* phase being energetically less preferred than the conventional Sm A* phase but requiring a lower activation energy barrier to be overcome, $E_A^{TGB} < E_A^{SmA}$. The model is supported with structural SAXS study of the both mesophases for same polymer sample at the same temperature but obtained with different cooling rates.

The cooling rate, r, affects strongly the transition point on subsequent heating, T_m. A linear dependence, $T_m \sim \ln r$, has been observed and explained theoretically for the raw polymer. In contrast, narrow polymer fractions show a kink at $r \sim 1$ K/min corresponding to the crossover above.

Finally, the suggested theoretical model for the "bistable phase behavior" is well confirmed by estimation of the activation energy of mesophase nuclei growth, E_A^{TGB} and E_A^{SmA}, as determined by a Kissinger analysis.

Acknowledgment. We are grateful to Dr. H. Pasch and Mr. Ch. Brinkman (DKI, Darmstadt) for the GPC−SEC measurements and to Mr. M. Roth (TU Darmstadt) for his assistance in DSC measurements. The work was supported by Deutsche Forschungsgemeinschaft (Projects Re 923/8 and Ha 782/74).

Supporting Information Available: Figures showing molecular model of mesogenic side chain in P8*NN (S1), suggested model for local Sm A packing of mesogenic side chains in P8*NN (S2), sketch of the twist grain boundary phase (S3), microphotograph of fiber drawn from P8*NN fraction 1 (S4), and 2D WAXS pattern from the fiber (S5). This material is available free of charge via the Internet at http://pubs.acs.org.

References and Notes

(1) Mandelkern, L. *Crystallization of Polymers,* 2nd ed.; Cambridge University Press: Cambridge, UK, 2002; 448 pp.
(2) Schultz, J. *Polymer Crystallization: The Development of Crystalline Order in Thermoplastic Polymers*, American Chemical Society: Washington, DC, 2001; 304 pp.
(3) Avrami, M. *J. Chem. Phys.* **1939**, *7*, 1103.
(4) Avrami, M. *J. Chem. Phys.* **1940**, *8*, 212.
(5) Pracella, M.; Frosini, V.; Galli, G.; Chiellini, E. *Mol. Cryst. Liq. Cryst.* **1984**, *113*, 201.
(6) Grebowicz, J.; Wunderlich, B. J. *J. Polym. Sci., Polym. Phys. Ed.* **1983**, *21*, 141.
(7) Liu, S. F.; Lee, Yu-D. *Macromol. Chem. Phys.* **1995**, *196*, 629.
(8) Cheng, S. Z. D. *Macromolecules* **1988**, *21*, 2475.
(9) Bhattacharya, S. K.; Misra, A.; Stein, R. S.; Lenz, R. W.; Hahn, P. E. *Polym. Bull. (Berlin)* **1986**, *16*, 465.
(10) Aharoni, S. M. *Macromolecules* **1989**, *22*, 1125.
(11) Galli, G.; McNamee, S. G.; Ober, C. K. *J. Polym. Sci., Polym. Phys. Ed.* **1993**, *31*, 773.
(12) Hans, K.; Zugenmeier, P. *Macromol. Chem.* **1988**, *189*, 1189.
(13) Kozlovsky, M. V.; Meier, J. G.; Stumpe, J. *Macromol. Chem. Phys.* **2000**, *201*, 2377.
(14) Kozlovsky, M. V. *J. Polym. Sci., Part B: Polym. Phys. Ed.* **2001**, *39*, 1055.
(15) Kozlovsky, M. *Cryst. Res. Technol.* **2001**, *36*, 1083.
(16) Ozawa, T. *Polymer* **1971**, *12*, 150.
(17) Cohen, L. E.; Rocco, A. M. *J. Therm. Anal. Calorim.* **2000**, *59*, 625.
(18) Lamberti, G.; Titomanlio, G. *Polym. Bull. (Berlin)* **2001**, *46*, 231.
(19) Bhattarai, N.; Kim, H. Y.; Il Cha, D.; Lee, D. R.; Il Yoo, D. *Eur. Polym. J.* **2003**, *39*, 1365.
(20) Benkhati, H.; Ton That Minh Tan; Jungnickel, B.-J. *J. Polym. Sci., Part B: Polym. Phys.* **2001**, *39* 2130.
(21) Kozlovsky, M. V.; Lymarenko, R. A.; Lu Wang; Haase, W. *Proc. SPIE* **2004**, *5521*, 85.

(22) Mandelkern, L. *Crystallization of Polymers*; McGraw-Hill: New York, 1964; p 323.
(23) Hoffman, J. D.; Weeks, J. J. *J. Res. Natl. Bur. Stand. A66*, 13.
(24) Kozlovsky, M. V.; Shibaev, V. P.; Stakhanov, A. I.; Weyrauch, T.; Haase, W. *Liq. Cryst.* **1998**, *24*, 759.
(25) Läsker, L.; Stumpe, J.; Fischer, T.; Rutloh, M.; Kostromin, S.; Ruhmann, R. *Mol. Cryst. Liq. Cryst. A* **1995**, *261*, 371.
(26) Schönhals, A.; Ruhmann, R.; Carius, H.-E.; Wolff, D. *Polym. Prepr.* **1997**, *38*, 429.
(27) Tsutsumi, O.; Miyashita, Y.; Hirano, S.; Shishido, A.; Kanazawa, A.; Shiono, T.; Ikeda, T. *Mol. Cryst. Liq. Cryst. A* **1998**, *312*, 33.
(28) Clingman, S. R.; Mao, G.; Ober, C. K.; Colby, R. H.; Brehmer, M.; Zentel, R.; Bignozzi, M.; Laus, M.; Angeloni, A.; Gillmor, J. R. *J. Polym. Sci., Polym. Phys.* **1999**, *37*, 405.
(29) Demikhov, E.; Kozlovsky, M. V. *Liq. Cryst.* **1995**, *18*, 911.
(30) Kozlovsky, M. V.; Demikhov, E. *Mol. Cryst. Liq. Cryst.* **1996**, *282*, 11.
(31) Kozlovsky, M. V.; Darius, M.; Haase, W. *Eur. Polym. J.* **1998**, *34*, 1629.
(32) Kozlovsky, M. *Liq. Cryst.*, in press
(33) Kozlovsky, M. V.; Haase, W. *Macromol. Symp.* **1999**, *137*, 47.
(34) Kozlovsky, M. V.; Meier, J. G.; Stumpe, J. *Macromol. Chem. Phys.* **2000**, *201*, 2377.
(35) Blinov, L. M.; Barberi, R.; Cipparrone, G.; Kozlovsky, M. V.; Lasarev, V. V.; Ozaki, M.; De Santo, M. P.; Scaramuzza, N.; Yoshino, K. *Mol. Cryst. Liq. Cryst.* **2001**, *355*, 359.
(36) Goodby, J. W.; Slaney, A. J.; Booth, C. J.; Nishiyama, I.; Vuijk, J. D.; Styring, P.; Toyne, J. *Mol. Cryst. Liq. Cryst.* **1994**, *243*, 231.
(37) Kitzerow, H.-S. In *Chirality in Liquid Crystals*; Kitzerow, H.-S., Bahr, Ch., Eds.; Springer: Berlin, 2000; p 296.
(38) Shibaev, V. P.; Freidzon, Ya. S. In *Side Chain Liquid Crystal Polymers*; McArdle, C. B., Ed.; Glasgow: Blackie, 1989; pp 260−286 and references therein.
(39) Cazé, C.; Devaux, E.; Crespy, A.; Cavrot, J. P. *Polymer* **1997**, *38*, 497.
(40) Cheng, S. Z. D.; Wunderlich, B. *Macromolecules* **1989**, *21*, 3327.
(41) Kissinger, H. E. *J. Res. Natl. Stand.* **1956**, *57*, 217.
(42) Vyazovkin, S.; Sbirrazzuoli, N. *Macromol. Rapid Commun.* **2002**, *23*, 766.
(43) Vyazovkin, S. *Macromol. Rapid Commun.* **2002**, *23*, 771.

MA047631O